

Photofragment Spectroscopy and Dynamics of NiOH⁺ and NiOH⁺(H₂O)

Christopher J. Thompson, Fernando Aguirre, John Husband, and Ricardo B. Metz*

Department of Chemistry, University of Massachusetts, Amherst, Massachusetts 01003

Received: May 23, 2000; In Final Form: September 11, 2000

Photodissociation of thermalized NiOH⁺ and NiOH⁺(H₂O) are examined over the visible and near-ultraviolet using time-of-flight mass spectrometry. Branching ratios and photodissociation cross sections are monitored as a function of laser wavelength. Loss of OH is the only dissociation channel observed in NiOH⁺, whereas loss of H₂O and OH are present, and competitive, in the photodissociation of NiOH⁺(H₂O). The photofragment spectrum of NiOH⁺ shows absorption bands at ~300 and ~400 nm. An almost identical spectrum is observed for the net photodissociation of NiOH⁺(H₂O). Spectroscopic thresholds taken from the photofragment spectra have been corrected to yield upper limits to the 0 K bond energies for the ions: $D^0_0(\text{Ni}^+-\text{OH}) \leq 271 \pm 9$ kJ/mol, $D^0_0(\text{NiOH}^+-\text{H}_2\text{O}) \leq 271 \pm 9$ kJ/mol, and $D^0_0(\text{Ni}^+\text{H}_2\text{O}-\text{OH}) \leq 334 \pm 5$ kJ/mol. Calculated B3LYP values are consistent with the experimental upper limits, but suggest that the true $D^0_0(\text{NiOH}^+-\text{H}_2\text{O})$ and $D^0_0(\text{Ni}^+\text{H}_2\text{O}-\text{OH})$ lie significantly below these upper limits. Photodissociation of NiOH⁺(H₂O) near 300 nm leads to greater OH production than RRKM calculations predict, suggesting that excitation in this region leads to direct Ni⁺-OH bond cleavage.

Introduction

Transition metal hydroxides (MOH⁺) are important components of diverse systems whose influence spans atmospheric, organometallic, and surface chemistries.^{1,2} In addition, solvated MOH⁺ species are frequently encountered in electrospray mass spectra, where they can be formed by charge reduction reactions of solvated dications:^{3,4}



The MOH⁺ species are quite intriguing, as they can be viewed as a combination of two limiting cases: either M⁺ bound to neutral OH, or M²⁺ ligated by OH⁻. As a result, the metal has a nominal charge between +1 and +2 and MOH⁺ typically binds water more strongly than bare M⁺. In a series of papers, Fuke and co-workers have used experiment and theory to investigate this effect in hydrated MgOH⁺ clusters.^{5,6} They demonstrate how the Mg⁺-H₂O bond is strengthened in (H₂O)MgOH⁺, as Mg⁺ is halfway oxidized to Mg²⁺ by OH.

Experimental work on transition metal MOH⁺ species has mainly focused on determining bond energies, rather than examining the effect of solvation on the spectroscopy of MOH⁺. Cassady and Freiser used deprotonation reactions and photodissociation to determine bond strengths and photofragment spectra of FeOH⁺ and CoOH⁺,⁷ while Michl and co-workers determined bond strengths for a variety of MOH⁺ species using collision-induced dissociation (CID).⁸ Recently, Armentrout and co-workers have more accurately measured these dissociation energies using endothermic ion-molecule reactions in a guided ion beam apparatus.⁹⁻¹¹ Complementing the experimental work, Bauschlicher and co-workers calculated M⁺-OH binding energies at both the CCSD(T) and B3LYP levels.¹² Also, Gilson and Krauss examined the absorption properties of solvated CoOH⁺, calculating the energies and oscillator strengths for the 10 lowest-lying electronic states of CoOH⁺(H₂O)_n ($n = 3-5$)

at the CAS-MCSCF and MCQDPT level.¹³ The hydrated CoOH⁺ ions were found to have modest absorptions near 440 nm. The transitions observed in the photofragment spectrum of bare CoOH⁺ are much more intense and lie at 340 nm and <250 nm and thus likely correspond to transitions beyond those calculated.

While there have been no experimental studies involving the effect of solvation on the spectroscopy of MOH⁺ species, Posey and co-workers have used photofragment spectroscopy to investigate solvation of ligated transition metal dications, where the ligands are neutral molecules.^{14,15} The effect of both the nature and number of solvent molecules on the strongly allowed ($\sigma = 2 \times 10^{-17}$ cm²) metal-to-ligand charge transfer (MLCT) band in molecules such as Fe²⁺(bpy)₃ and Fe²⁺(terpy)₂ were studied. These studies reveal photofragment spectra that are similar to, but slightly shifted from, solution absorption spectra, implying that the oxidation state of the metal in solution is retained in the gas phase.¹⁶

Our group has studied the effect of solvation on hydrated M²⁺, determining absorption properties and dissociation dynamics of M²⁺(H₂O)_n (M = Co, Ni; $n = 4-7$).^{17,18} In this work, we examine the photofragment spectroscopy of thermalized NiOH⁺ and how it is influenced by the presence of a solvent water molecule.

Experimental Section

The experimental apparatus has been described in detail elsewhere,^{17,19} so only a succinct description will be given here. NiOH⁺ and NiOH⁺(H₂O) are produced using a home-built electrospray source in which a solution of 3.0×10^{-4} M NiCl₂ in distilled water is delivered at a rate of 0.3 mL/h to the spray needle, typically held at 7 kV. Ions enter the interface chamber through a heated capillary, pass through a skimmer, and are led by an octopole ion guide into a quadrupole RF ion trap. Ions are trapped for a maximum of 49 ms and thermalized to 300 K by approximately 900 collisions with ~1 mTorr helium and 300 collisions with ~0.3 mTorr air. A pulsed electric field

* Author to whom all correspondence should be addressed. E-mail: rbmetz@chemistry.umass.edu.

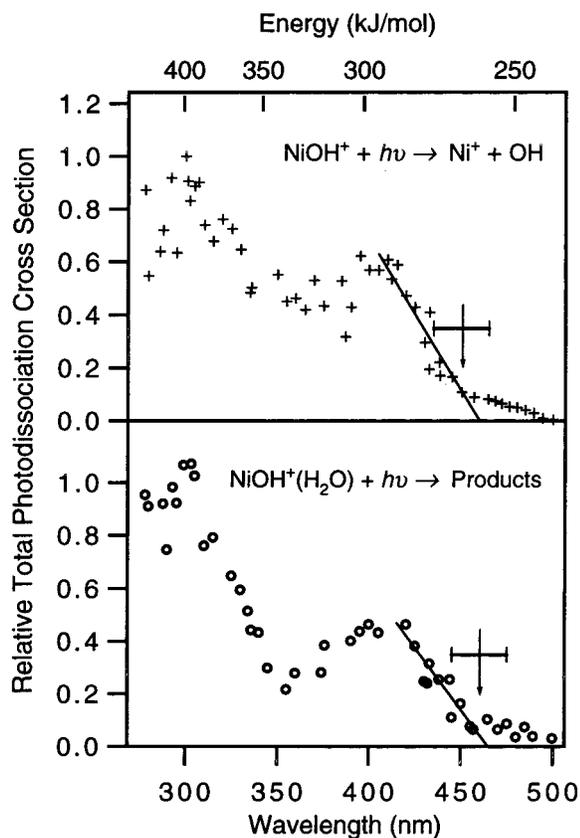


Figure 1. Photofragment spectra of NiOH^+ and $\text{NiOH}^+(\text{H}_2\text{O})$. The top spectrum shows the photodissociation of NiOH^+ to $\text{Ni}^+ + \text{OH}$ as a function of dissociation laser wavelength. The vertical arrow at 450 nm and ± 15 nm error bars indicate the spectroscopic onset for photodissociation. It is assigned as the wavelength where the long-wavelength edge of the photofragment spectrum (line in the figure) intersects the tail due to photodissociation of internally excited ions. The bottom spectrum shows the total photofragment spectrum of $\text{NiOH}^+(\text{H}_2\text{O})$ obtained by summing dissociation to the two observed channels (loss of H_2O , loss of OH). The vertical arrow at 460 ± 15 nm indicates the spectroscopic dissociation onset. A relative cross section of 1 corresponds to $\sigma \approx 1.4 \times 10^{-17} \text{ cm}^2$ in all figures.

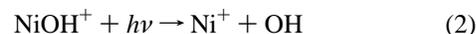
extracts trapped ions which are subsequently accelerated to 1800 V, re-referenced to ground potential, mass selected, and deflected into the reflectron time-of-flight mass spectrometer.

To obtain photofragment spectra from 275 to 500 nm, the second or third harmonic of a pulsed (20 Hz) Nd:YAG laser pumps a dye laser whose output is either doubled, mixed with 1064 nm light, or used unaltered. Excitation of mass-selected ions occurs at the turning point of the reflectron using the unfocused laser beam. Multiphoton effects are minimized by attenuating the excitation laser to keep dissociation below 15%. Parent and fragment ions reaccelerate as they leave the reflectron and their flight times and intensities are determined using a 40 mm diameter dual microchannel plate detector. Fragment channels and branching ratios are monitored through *difference spectra*—the difference between mass spectra obtained with the photodissociation laser blocked and unblocked. *Photofragment action spectra*—the absorption spectra of those ions that dissociate to give a particular fragment—are obtained by monitoring the total yield of a fragment ion as a function of wavelength and normalizing to parent signal and laser fluence.

Results and Discussion

Photofragment Spectra. Photofragment spectra of NiOH^+ and $\text{NiOH}^+(\text{H}_2\text{O})$ are obtained from 275 to 500 nm. In the case

of NiOH^+ , photodissociation of the ion occurs exclusively via loss of OH :



Fragmentation by loss of OH and known Ni^+-H and Ni^+-OH thermochemistry²⁰ imply NiOH^+ , not HNiO^+ , is the parent species being studied. The photofragment spectrum of NiOH^+ is shown in the top of Figure 1 and reveals absorption maxima at ~ 300 and ~ 400 nm with absolute cross sections $\sigma = 1.4 \times 10^{-17}$ and $9 \times 10^{-18} \text{ cm}^2$, respectively. Uncertainties are estimated at 50% for absolute cross sections and 20% for relative cross sections and are due to laser beam nonuniformity and the overlap between the laser and ion beams.^{17,19} Narrow wavelength scans taken throughout the range studied reveal no sharp structure.

While there have been no previously reported spectroscopic studies of NiOH^+ , Cassady and Freiser have obtained photofragment spectra for FeOH^+ and CoOH^+ .⁷ The FeOH^+ spectrum resembles that of NiOH^+ , with maxima at 290 and 330 nm. CoOH^+ differs from both NiOH^+ and FeOH^+ in that only one peak is observed, at 340 nm. Additionally, the onset for photodissociation in NiOH^+ occurs near 450 nm, whereas FeOH^+ and CoOH^+ only dissociate below 400 nm. This trend is consistent with weaker bonding by Ni^+ than Fe^+ and Co^+ .¹¹ All three MOH^+ species exhibit similar absorption intensities, having cross sections on the order of $3\text{--}8 \times 10^{-18} \text{ cm}^2$ for FeOH^+ and CoOH^+ ,⁷ and $9\text{--}14 \times 10^{-18} \text{ cm}^2$ for NiOH^+ . Comparison to other systems shows that the MOH^+ bands are nearly as intense as the MLCT bands studied by Posey and co-workers,^{14,15} and are two to three orders of magnitude more intense than the visible bands of $\text{M}^{2+}(\text{H}_2\text{O})_n$ ($\text{M} = \text{Co}, \text{Ni}; n = 4\text{--}7$).^{17,18}

Photofragmentation of $\text{NiOH}^+(\text{H}_2\text{O})$ occurs by two pathways:

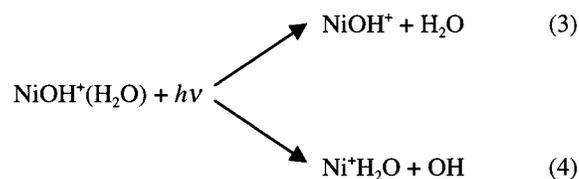


Figure 1 compares the overall dissociation of $\text{NiOH}^+(\text{H}_2\text{O})$ to that of NiOH^+ . Clearly, the total photofragment spectrum of $\text{NiOH}^+(\text{H}_2\text{O})$ is very similar to that of NiOH^+ . The similarities of the two spectra imply that the strongly absorbing NiOH^+ is the chromophore in $\text{NiOH}^+(\text{H}_2\text{O})$. Solvation slightly changes the peak intensities and only leads to minor shifts in the peak maxima. Shifts in each absorption band are determined by overlaying the spectra of the two molecules and varying the x -axis of one until the peaks match. The presence of a water molecule shifts the 400 nm band by at most 5 nm to the red and the low-energy onset of the 300 nm band by approximately 5 nm to the blue. Photofragment spectra of $\text{NiOH}^+(\text{H}_2\text{O})$ obtained for individual dissociation channels are given in Figure 2. In the 400 nm band, photodissociation occurs overwhelmingly by loss of H_2O . Loss of OH occurs only below 370 nm, and becomes the primary dissociation pathway below ~ 330 nm.

Observed spectroscopic thresholds to dissociation for each channel give an upper bound to the corresponding bond strength. Collisions due to extraction from the ion trap result in a small amount of vibrationally excited ions that give rise to the dissociation tails extending to 500 nm in Figure 1. The onset for dissociation of thermalized NiOH^+ by reaction 2 is assigned to 450 ± 15 nm by extrapolating the primary slope of the 400

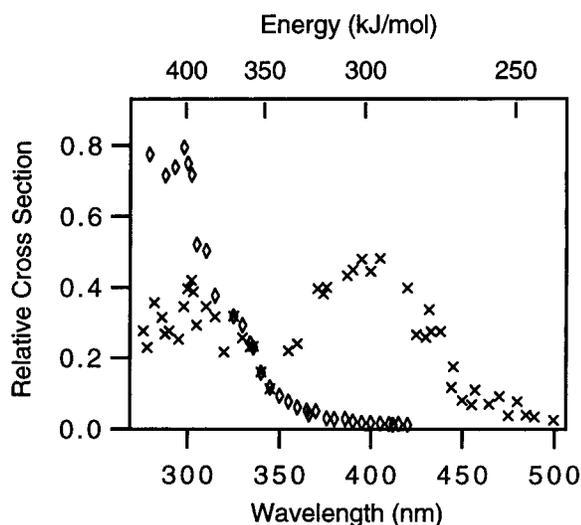


Figure 2. Individual channels in the photofragment spectrum of NiOH⁺(H₂O). Dissociation to NiOH⁺ + H₂O (x) is the dominant pathway until 330 nm when dissociation to Ni⁺H₂O + OH (◇) becomes the preferred dissociation channel.

TABLE 1: Experimental and Calculated Ionization and Dissociation Energies of Nickel-containing Species^a

	this work		literature	
	calcd	expt	calcd	expt
IE(Ni)	781		778 ^b	737.1 ^e
IE(Ni ⁺)	1778			1751.2 ^e
$D^0_0(\text{Ni}^+-\text{OH})$	261	$\leq 271 \pm 9$	250 ^c	$235 \pm 19^f, 168 \text{ g}$
$D^0_0(\text{Ni}^+-\text{H}_2\text{O})$	180		172 ^d	180 ± 3^h
$D^0_0(\text{NiOH}^+-\text{H}_2\text{O})$	212	$\leq 271 \pm 9$		
$D^0_0(\text{Ni}^+\text{H}_2\text{O}-\text{OH})$	292	$\leq 334 \pm 5$		

^a All values are given in kJ/mol and correspond to 0 K. ^b From ref 24. ^c From ref 12. ^d From ref 27. ^e From ref 25. ^f From ref 11. ^g From ref 8. ^h From ref 26.

nm band to the intersection with the tail, as shown in Figure 1. As threshold photodissociation of thermalized parent ions produces internally cold fragments,^{11,21} the observed onset needs to be corrected to 0 K. Applied thermal shifts are determined using the vibrational frequencies and rotational contributions of the parent species as described by Armentrout and Kickel.¹¹ Gaussian98²² calculations (described in detail below) were used to determine the vibrational frequencies, which are available as Supporting Information (Table 1S). Including the vibrational and rotational energies of the parent ion leads to a 5 kJ/mol shift, giving a 0 K *upper limit* to the Ni⁺-OH bond strength of $D^0_0 \leq 271 \pm 9$ kJ/mol. Clemmer and Armentrout¹¹ used ion beam experiments to determine the bond strength $D^0_0(\text{Ni}^+-\text{OH}) = 235 \pm 19$ kJ/mol, in agreement with our upper bound. Similarly, for NiOH⁺(H₂O), we assign upper limit bond strengths $D^0_0(\text{NiOH}^+-\text{H}_2\text{O}) \leq 271 \pm 9$ kJ/mol and $D^0_0(\text{Ni}^+\text{H}_2\text{O}-\text{OH}) \leq 334 \pm 5$ kJ/mol. These values include a thermal shift of 11 kJ/mol from the observed spectroscopic thresholds of 460 ± 15 nm and 370 ± 5 nm, respectively.

Calculations. The similarities between the absorption properties of NiOH⁺ and NiOH⁺(H₂O) suggest that NiOH⁺ is the chromophore for NiOH⁺(H₂O). It is likely then that the 460 nm onset to reaction 3 is a spectroscopic threshold, which reflects the absorption properties of the NiOH⁺ chromophore, rather than a thermodynamic threshold that indicates the minimum energy required for dissociation. To this end, hybrid density functional calculations have been performed to gain some insight into how close the experimental upper bounds are to the true bond strengths. Optimized geometries, single-point

energies, and vibrational frequencies of NiOH⁺, NiOH(H₂O)⁺, and their photoproducts were calculated using the B3LYP hybrid density functional method. All calculations were performed using Gaussian98²² running on a 500 MHz Pentium III. The diffuse 6-311+(3df,2pd) basis set was used on oxygen and hydrogen, while the Stuttgart/Dresden quasirelativistic effective core potential (ECP) basis set was used on nickel. Basis sets and ECPs were used unmodified from the standard forms in Gaussian98. A survey of the literature suggests that the method employed here will yield reasonably accurate results: bond energies of iron-containing compounds have been shown to have RMS errors of less than 15 kJ/mol with no systematic error detected,²³ while the ionization potential of Ni was shown to have a mean absolute deviation of 17 kJ/mol.²⁴ Thus, we can expect calculated bond strengths to be accurate to within approximately 15 kJ/mol.

The results of preliminary calculations, done in order to assess the reliability of the method, are listed in Table 1. All of the calculated bond strengths have been corrected for zero-point energy and correspond to 0 K values. No vibrational scaling factors have been used. Good agreement is found between calculated ionization energies and reported experimental values.²⁵ Additionally, the calculated dissociation energy for Ni⁺-H₂O is in excellent agreement with both the experimental value of Armentrout and co-workers,^{11,26} and the self-consistent-field value given by Rosi and Bauschlicher.²⁷

Calculations also demonstrate the strong polarizing effect that OH has on Ni⁺. In the presence of OH, the nominal charge on the metal cation is raised to +1.3. The molecular ion, NiOH⁺, is then found to bind H₂O 18% more strongly than bare Ni⁺, as is shown in Table 1. Thus, the electrostatic attraction to H₂O is increased in NiOH⁺ over Ni⁺. A similar effect can be seen in the work of Fuke and co-workers on hydrated MgOH⁺ species.^{5,6} They calculated an almost 50% increase in H₂O binding in MgOH⁺ over Mg⁺. The dramatic increase in electrostatic binding in the Mg⁺ case is a result of the OH halfway oxidizing the cation to Mg²⁺.

Having converted experimental bond strengths to 0 K values, a direct comparison can be made between observed photodissociation thresholds and calculated values. For Ni⁺-OH, the computed dissociation energy of 261 kJ/mol agrees with our experimentally determined upper limit of 271 ± 9 kJ/mol. The observed upper bound is thus probably close to the true dissociation energy. The calculation clearly favors $D^0_0(\text{Ni}^+-\text{OH}) = 235 \pm 19$ kJ/mol obtained in the ion beam experiments of Clemmer and Armentrout¹¹ over the earlier CID value of $D^0_0(\text{Ni}^+-\text{OH}) = 168 \pm 12$ kJ/mol measured by Michl and co-workers.⁸

In the case of NiOH⁺(H₂O), the calculated dissociation energies for each channel lie ~ 50 kJ/mol below the experimental upper limits. This discrepancy is probably due to either spectroscopic or dynamical factors, as the calculated values should be accurate to 15 kJ/mol. The delayed onset of dissociation via the low-energy channel, loss of H₂O, is probably due to lack of absorption between the calculated thermodynamic onset of 564 nm and our observed onset of 460 nm. However, the shift in the high-energy OH loss channel is obviously not due to a lack of absorption, but could rather be due to dynamics: competition between OH loss and the less endothermic H₂O loss.

Photodissociation Dynamics. Let us examine the branching between the two channels further. Figure 3 shows the ratio of the two dissociation channels in NiOH⁺(H₂O). Even though NiOH⁺(H₂O) is a small molecule and NiOH⁺ is clearly the

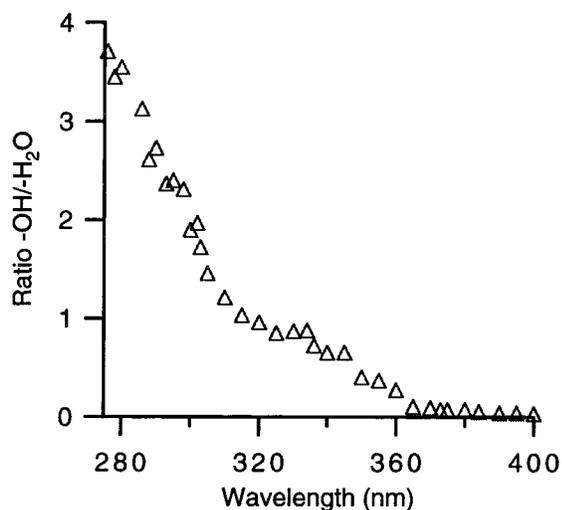


Figure 3. Ratio of OH loss to H₂O loss in the photodissociation of NiOH⁺(H₂O).

chromophore, the smooth change in the ratio suggests that the competitive dissociation may be statistical. To test this idea, the unimolecular dissociation rate of NiOH⁺(H₂O) to each fragment channel was calculated using the Phase Space Limit (PSL) RRKM theory.^{28–30} This method has proven successful in modeling competitive dissociation channels in CID experiments. On the basis of this theory, the transition state (TS) for dissociation to NiOH⁺ + H₂O was assumed to be loose, which is appropriate for a complex held together by ion–dipole forces. Therefore, most of the molecular parameters for the TS were taken from the products. Product vibrational frequencies were used for the TS frequencies, while product rotations were treated as hindered rotations in the TS. As arguments could be made for treating dissociation to form Ni⁺H₂O + OH with either a loose or a tight TS, both approaches were tried. The density of ro-vibrational states in NiOH⁺(H₂O) and in each TS was evaluated using the Beyer–Swinehart algorithm.^{31,32} Before attempting an in-depth analysis of this competition, we use the following thermodynamic relation to simplify the calculation:

$$D^{\circ}_0(\text{Ni}^+\text{H}_2\text{O}-\text{OH}) + D^{\circ}_0(\text{Ni}^+-\text{H}_2\text{O}) = D^{\circ}_0(\text{NiOH}^+-\text{H}_2\text{O}) + D^{\circ}_0(\text{Ni}^+-\text{OH}) \quad (5)$$

Using calculated bond strengths, the two dissociation channels in NiOH⁺(H₂O) are predicted to lie 82 kJ/mol apart, with the loss of water being the lower channel.

So, from the above thermochemical cycle, the energy spacing between dissociation channels was fixed to be 82 kJ/mol in the RRKM calculations. Unscaled RRKM calculations were unable to fit the experimental data, implying that the competitive process is *not* statistical. The RRKM results obtained using a loose TS for both channels and the calculated value of $D^{\circ}_0(\text{NiOH}^+-\text{H}_2\text{O})$ needed to be scaled by a factor of 150, while using a tight TS for loss of H₂O requires a scaling factor of 400000 to fit the experimental data. Varying $D^{\circ}_0(\text{NiOH}^+-\text{H}_2\text{O})$ or the energy difference between the two dissociation channels by ± 40 kJ/mol still requires large scaling factors for the RRKM calculations to fit the experimental data.

An understanding of the nature of the competitive dissociation of NiOH⁺(H₂O) can be gained by comparing the spectra shown in Figure 1. There are two absorption bands in the photofragment spectra of NiOH⁺ and NiOH⁺(H₂O), indicating excitation to at least two distinct electronic states of the NiOH⁺ chromophore. Figure 3 shows that excitation of the 400 nm band of

NiOH⁺(H₂O) leads overwhelmingly to loss of water, although the calculations suggest that loss of OH is energetically allowed below 426 nm. It is likely that loss of H₂O is the only channel observed in this wavelength region because the initially excited state is sufficiently long-lived to redistribute energy prior to dissociation, and statistical dissociation clearly favors loss of H₂O. On the other hand, exciting the 300 nm band preferentially leads to loss of OH. This nonstatistical result is likely due to rapid dissociation of the (H₂O)Ni⁺–OH bond following excitation of the NiOH⁺ chromophore. In an elegant series of photodissociation studies of bromo-iodo-hydrocarbons, Butler, Lee and co-workers quantified a similar effect, the preferential cleavage of an initially excited C–Br bond rather than a weaker C–I bond.^{33–35}

Excited Electronic States—A Molecular Orbital Picture. Qualitatively similar spectra to NiOH⁺ are seen in FeOH⁺ and CoOH⁺,⁷ as well as FeCO⁺,⁷ NiS⁺, and FeS⁺,^{36,37} suggesting that the electronic transitions arise from a similar mechanism. The number of unpaired electrons and low-lying orbitals make these systems very challenging for theory, especially at the high energies typical of photofragmentation experiments. To try to identify the states responsible for the observed bands, we proceed by analogy with metal oxides and fluorides, both neutrals and cations, which are more thoroughly understood. Thus, we ignore the influence of the hydrogen atom and treat MOH⁺ as a pseudodiatom ML⁺. The extensive theoretical work on transition metal–main group diatomics has been nicely summarized by Harrison,³⁸ while Merer’s detailed review³⁹ focuses on the metal oxides.

A simple molecular orbital picture has been used by several authors (see refs 38–40 and references therein) to qualitatively describe *neutral* MO and MF, where M is a late-first-row transition metal. In this view, the ligand 2p_z and metal 4s and 3d_z orbitals form the 8σ, 9σ, and 10σ molecular orbitals. Combining the ligand 2p_{x,y} orbitals with the metal 3dπ forms the doubly degenerate 3π and 4π orbitals; the metal 3dδ become the doubly degenerate 1δ orbital. The higher-lying metal 4p orbitals give rise to the 11σ and 5π orbitals. The lowest-lying valence orbitals, 8σ and 3π, are bonding, with most of the electron density on the ligand. Above these are the nonbonding 1δ and 9σ and the higher-lying 4π and 10σ antibonding orbitals, which are primarily metal-centered. The nonbonding 5π molecular orbital retains metal 4p character, stabilized by interaction with the ligand, while the 11σ is destabilized as a result of its interaction with the 10σ.^{40,41} NiO, which is isoelectronic with NiOH⁺, has a ³Σ[−] ground state with an orbital occupancy of ... (8σ)²(3π)⁴(1δ)⁴(9σ)²(4π)²(10σ)⁰.⁴² While the visible spectrum of NiO is extremely complex and poorly understood, transitions from the 8σ and 3π molecular orbitals to the 10σ* have been observed in several neutral metal oxides and occur at energies below 20000 cm^{−1}.^{39,43} In the corresponding cations, the increased charge on the metal causes its orbitals to drop in energy relative to the ligand 2p orbital. The resulting molecular orbitals have a similar order to those in the neutral systems, but the nature of the orbitals changes, with the lower orbitals (8σ and 3π) having more metal character and the higher-lying orbitals having more ligand character than in the neutrals. In one of the few cationic systems assigned to date, Brucat and co-workers observe the 3π → 10σ* charge-transfer transition in CoO⁺ near 17 000 cm^{−1}.⁴⁴

Several of the bands observed in MOH⁺ are at significantly higher energy and thus likely correspond to transitions to the higher-lying 5π orbital. This is supported by calculations on FeF which indicate that the strong bands observed near 30000

cm⁻¹ are based on promotions to the 5π molecular orbital, while transitions to the 11σ orbitals are calculated to occur above 50000 cm⁻¹.^{40,41} Although transitions to the 4p orbital in the bare metal ion are at higher energies, 3d⁸4s (²F) → 3d⁸4p (²G) in Ni⁺ is at 41 750 cm⁻¹,²⁵ interaction with the ligand will lower the transition energy.^{45,46} The MOH⁺ bands are quite intense and fairly broad. For example, the 400 nm band of NiOH⁺ has an oscillator strength $f = 0.03$ and $\text{fwhm} \approx 3000 \text{ cm}^{-1}$. The observed intensity is consistent with a promotion from a molecular orbital with substantial metal 3d or 4s character to one with metal 4p character, or with a charge-transfer transition from a ligand-based orbital to a metal 4p-based orbital.

Conclusions

Thermalized NiOH⁺ and NiOH⁺(H₂O) have been generated using an electrospray ion source and photofragment action spectra were obtained for both species from 275 to 500 nm. Comparisons of photofragment spectra show that NiOH⁺ is the active chromophore in both species, with cross sections comparable to those of FeOH⁺ and CoOH⁺. Spectroscopic thresholds taken from the spectra have been corrected to yield the following 0 K upper limits to the bond strengths: $D^0_0(\text{Ni}^+ - \text{OH}) \leq 271 \pm 9 \text{ kJ/mol}$, $D^0_0(\text{NiOH} - \text{H}_2\text{O}) \leq 271 \pm 9 \text{ kJ/mol}$, and $D^0_0(\text{Ni}^+\text{H}_2\text{O} - \text{OH}) \leq 334 \pm 5 \text{ kJ/mol}$. Calculated B3LYP dissociation energies agree with the experimental upper limits. NiOH⁺(H₂O) dissociates by loss of H₂O and, below 370 nm, OH. The relative yield of OH steadily increases with energy, and OH loss dominates below 330 nm. Unscaled RRKM calculations are unable to fit the experimental data, implying that the competitive process is not statistical. Rather, the preferential dissociation is a result of the state to which the NiOH⁺ chromophore is excited. Loss of H₂O near 400 nm is due to a relatively long-lived excited state, while loss of OH near 300 nm is the result of excitation to a rapidly dissociative state.

Acknowledgment. The authors thank Dr. J. Fermann and Prof. S. Auerbach for their assistance with the computational efforts. Support of this work by a National Science Foundation Faculty Early Career Development Award and by the donors of the Petroleum Research Fund, administered by the American Chemical Society, is gratefully acknowledged.

Supporting Information Available: Single point energies, vibrational frequencies, and rotational constants of the species listed in Table 1, and their resulting photoproducts. This material is available free of charge via the Internet at <http://pubs.acs.org>.

References and Notes

- Duncan, M. A. *Annu. Rev. Phys. Chem.* **1997**, *8*, 69–93.
- Eller, K.; Schwarz, H. *Chem. Rev.* **1991**, *91*, 1121–1177.
- Blades, A. T.; Jayaweera, P.; Ikononou, M. G.; Kebarle, P. *Int. J. Mass Spectrom.* **1990**, *102*, 251–267.
- Agnes, G. R.; Horlick, G. *Appl. Spectrosc.* **1994**, *48*, 655–661.
- Sanekata, M.; Misaizu, F.; Fuke, K.; Iwata, S.; Hashimoto, H. *J. Am. Chem. Soc.* **1995**, *116*, 747–754.
- Watanabe, H.; Iwata, S.; Hashimoto, K.; Misaizu, F.; Fuke, K. *J. Am. Chem. Soc.* **1995**, *117*, 755–763.
- Cassady, C. J.; Freiser, B. S. *J. Am. Chem. Soc.* **1984**, *106*, 6176–6179.
- Magnera, T. F.; David, D. E.; Michl, J. *J. Am. Chem. Soc.* **1989**, *111*, 4100–4101.
- Clemmer, D. E.; Aristov, N.; Armentrout, P. B. *J. Phys. Chem.* **1993**, *97*, 544–552.
- Chen, Y.-M.; Clemmer, D. E.; Armentrout, P. B. *J. Am. Chem. Soc.* **1994**, *116*, 7815–7826.
- Armentrout, P. B.; Kickel, B. L. Gas-phase thermochemistry of transition metal ligand systems: reassessment of values and periodic trends. In *Organometallic Ion Chemistry*; Freiser, B. S., Ed.; Kluwer Academic Publisher: Dordrecht, 1996; pp 1–45.
- Ricca, A.; Bauschlicher, C. W., Jr. *J. Phys. Chem. A* **1997**, *101*, 8949–8955.
- Gilson, H. S. R.; Krauss, M. *J. Phys. Chem. A* **1998**, *102*, 6525–6532.
- Spence, T. G.; Trotter, B. T.; Burns, T. D.; Posey, L. A. *J. Phys. Chem. A* **1998**, *102*, 6101–6106.
- Spence, T. G.; Burns, T. D.; Guckenberger, G. B.; Posey, L. A. *J. Phys. Chem. A* **1997**, *101*, 1081–1092.
- Burns, T. D.; Spence, T. G.; Mooney, M. A.; Posey, L. A. *Chem. Phys. Lett.* **1996**, *258*, 669–679.
- Thompson, C. J.; Husband, J.; Aguirre, F.; Metz, R. B. *J. Phys. Chem. A* **2000**, *104*, 8155–8159.
- Faherty, K. P.; Thompson, C. J.; Aguirre, F.; Metz, R. B. In preparation.
- Husband, J.; Aguirre, F.; Ferguson, P.; Metz, R. *J. Chem. Phys.* **1999**, *111*, 1433–1437.
- Organometallic Ion Chemistry*; Freiser, B. S., Ed.; Kluwer Academic Publishers: Dordrecht, 1996.
- Aguirre, F.; Husband, J.; Thompson, C. J.; Metz, R. B. *Chem. Phys. Lett.* **2000**, *318*, 466–470.
- Frisch, M. J.; Trucks, G. W.; Schlegel, H. B.; Scuseria, G. E.; Robb, M. A.; Cheeseman, J. R.; Zakrzewski, V. G.; Montgomery, J. A.; Stratmann, R. E.; Burant, J. C.; Dapprich, S.; Millam, J. M.; Daniels, A. D.; Kudin, K. N.; Strain, M. C.; Farkas, O.; Tomasi, J.; Barone, V.; Cossi, M.; Cammi, R.; Mennucci, B.; Pomelli, C.; Adamo, C.; Clifford, S.; Ochterski, J.; Petersson, G. A.; Ayala, P. Y.; Cui, Q.; Morokuma, K.; Malick, D. K.; Rabuck, A. D.; Raghavachari, K.; Foresman, J. B.; Cioslowski, J.; Ortiz, J. V.; Stefanov, B. B.; Liu, G.; Liashenko, A.; Piskorz, P.; Komaromi, I.; Gomperts, R.; Martin, R. L.; Fox, D. J.; Keith, T.; Al-Laham, M. A.; Peng, C. Y.; Nanayakkara, A.; Gonzalez, C.; Challacombe, M.; Gill, P. M. W.; Johnson, B. G.; Chen, W.; Wong, M. W.; Andres, J. L.; Head-Gordon, M.; Replogle, E. S.; Pople, J. A. *Gaussian 98*, Revision A.3; Gaussian, Inc.: Pittsburgh, PA, 1998.
- Glukhovtsev, M. N.; Bach, R. B.; Nagel, C. J. *J. Phys. Chem. A* **1997**, *101*, 316–323.
- Yanagisawa, S.; Tsuneda, T.; Hirao, K. *J. Chem. Phys.* **2000**, *112*, 545–553.
- Sugar, J.; Corliss, C. *J. Phys. Chem. Ref. Data* **1985**, *14*, Suppl. 2.
- Dalleska, N. F.; Honma, K.; Sunderlin, L. S.; Armentrout, P. B. *J. Am. Chem. Soc.* **1994**, *116*, 9–3528.
- Rosi, M.; Bauschlicher, C. W., Jr. *J. Chem. Phys.* **1990**, *92*, 1876–1878.
- Rodgers, M. T.; Ervin, K. M.; Armentrout, P. B. *J. Chem. Phys.* **1997**, *106*, 4499–4508.
- Rodgers, M. T.; Armentrout, P. B. *J. Phys. Chem. A* **1999**, *103*, 4955–4963.
- Spasov, V. A.; Lee, T. H.; Maberry, J. P.; Ervin, K. M. *J. Chem. Phys.* **1999**, *110*, 5208–5217.
- Stein, S. E.; Rabinovitch, B. S. *J. Chem. Phys.* **1973**, *58*, 2438–2445.
- Stein, S. E.; Rabinovitch, B. S. *Chem. Phys. Lett.* **1977**, *49*, 183–188.
- Butler, L. J.; Hints, E. J.; Shane, S. F.; Lee, Y. T. *J. Chem. Phys.* **1987**, *86*, 2051–2074.
- Stevens, J. E.; Kitchen, D. C.; Waschewsky, G. C. G.; Butler, L. J. *J. Chem. Phys.* **1995**, *102*, 3179–3187.
- Butler, L. J. *Annu. Rev. Phys. Chem.* **1998**, *49*, 125–171.
- Hettich, R. L.; Jackson, T. C.; Stanko, E. M.; Freiser, B. S. *J. Am. Chem. Soc.* **1986**, *108*, 5086–5093.
- Husband, J.; Aguirre, F.; Metz, R. B. In preparation.
- Harrison, J. F. *Chem. Rev.* **2000**, *100*, 679–716.
- Merer, A. J. *Annu. Rev. Phys. Chem.* **1989**, *40*, 407–438.
- Pouilly, B.; Schamps, J.; Lumley, D. J. W.; Barrow, R. F. *J. Phys. B: Atom. Mol. Phys.* **1978**, *11*, 2281–2287.
- Pouilly, B.; Schamps, J.; Lumley, D. J. W.; Barrow, R. F. *J. Phys. B: Atom. Mol. Phys.* **1978**, *11*, 2289–2299.
- Bauschlicher, C. W., Jr.; Maitre, P. *Theor. Chim. Acta* **1995**, *90*, 189–203.
- Green, K. M.; Kampf, R. P.; Parson, J. M. *J. Chem. Phys.* **2000**, *112*, 1721–1732.
- Kamariotis, A.; Hayes, T.; Bellert, D.; Brucat, P. J. *Chem. Phys. Lett.* **2000**, *316*, 60–66.
- Field, R. W. *Ber. Bunsen-Ges. Phys. Chem.* **1982**, *86*, 771–779.
- Kaledin, L. A.; McCord, J. E.; Heaven, M. C. *J. Mol. Spectrosc.* **1995**, *173*, 499–509.